remote sensing

MDPI

Article

Forward Scatter Radar Meets Satellite: Passive Sensing of Aerial Target Using Satellite Communication Waveforms

Mingqian Liu [1], Zhenju Zhang [1,*], Yunfei Chen [2], Shifei Zheng [1] and Jianhua Ge [1]

[1] State Key Laboratory of Integrated Service Networks, Xidian University, Xi'an 710071, China; mqliu@mail.xidian.edu.cn (M.L.); zhangjl@stu.xidian.edu.cn (S.Z.); jhge@xidian.edu.cn (J.G.)
[2] School of Engineering, University of Warwick, Coventry CV4 7AL, UK; yunfei.chen@warwick.ac.uk
* Correspondence: zhenjuzhang@stu.xidian.edu.cn

Abstract: The problem of single-channel reception of global positioning system (GPS) communication waveforms makes passive sensing of aerial target difficult because of forward scatter. This paper proposes a novel aerial target passive sensing method based on linear canonical transformation (LCT) using the forward scattered satellite communication waveforms. The proposed method firstly preprocesses the received signal based on the characteristics of the traditional satellite tracking loop and the forward scattered satellite communication waveforms to effectively suppress the interference of the direct wave through DC removal. Then, the Gaussian noise and multipath interference in the channel are suppressed by applying a rectangular window to its linear canonical domain. Finally, aerial target sensing is performed based on the peak value of signals in the linear canonical transform domain. The characteristic signal is constructed by analyzing the satellite communication waveforms. Combining the linear canonical transform with the matched filter (MF) to estimate the target parameter. Simulation results show that the proposed method can effectively perform the aerial target sensing by using satellite communication waveforms in the forward scatter scenario.

Keywords: forward scatter; target parameter estimation; target passive sensing; satellite communication waveforms

Citation: Liu, M.; Zhang, Z.; Chen, Y.; Zheng, S.; Ge, J. Forward Scatter Radar Meets Satellite: Passive Sensing of Aerial Target Using Satellite Communication Waveforms. *Remote Sens.* **2022**, *14*, 1375. https://doi.org/10.3390/rs14061375

Academic Editors: Dmitriy Garmatyuk and Chandra Sekhar Pappu

Received: 26 January 2022
Accepted: 9 March 2022
Published: 11 March 2022

1. Introduction

Passive sensing systems generally use the electromagnetic waves of external radiation source, such as FM broadcast, satellite, digital TV broadcast, etc. It has many advantages, such as anti-stealth, strong survivability, low cost, and not affected by active directional interference; however, the power of the receiver is insufficient for effective target sensing in many cases [1,2]. Among many external radiation sources for passive sensing, satellite communication waveforms have high coverage and availability. Thus, target sensing based on satellite communication waveforms has great potential [3,4].

Forward scatter radar is a bistatic radar configuration with a special geometry, in which the target is located between the transmitter and the receiver. This means that the bistatic angle is close to 180° [5]. Compared with conventional radar systems, its main characteristics is scattering. In addition, the radar cross section (RCS) of the target is high in the case of forward scatter [6]. If the moving target crosses the baseline, it is easier to sense target. This allows the forward scatter radar to use satellites as sources of illumination to sense the target. Meanwhile, although the forward scatter area is very narrow, the richness of the satellite and the convenient handling of the receiver make the satellite forward scatter radar capable of sensing aerial target in a wide area.

Many works have been conducted on forward scatter radar (FSR) [7–10]. In particular, there has been progress on the sensing of ground, sea, and aerial targets by the forward scatter radar. For ground target sensing, R. Abdullah et al. constructed a forward scatter system based on the power spectrum difference generated when crossing the baseline [11]. For marine target sensing, transmitters and receivers were set up on both sides of the strait

to sense ships that cross the baseline, and echoes with large differences were observed [12]. Reference [13–16] used machine learning to detect and classify targets, which improved the efficiency of target detection of synthetic aperture radar (SAR). Since the satellite has a low receiving power, and the FSR system has a large radar cross-sectional area, the use of satellites as external radiation sources to construct FSR systems for the aerial target sensing is also one of the important areas of FSR systems. In [17], the characteristics of the forward-scattered GPS signals were studied when the aircraft crossed the vertical baseline. Numerical results demonstrated that the height of the target crossing the highest point, the azimuth, speed, and other factors from the receiver had considerable impact on the amplitude of the received signals.

The use of satellites as forward scatter radars for passive sensing of aerial targets was studied in [18,19]. In [20], the method for extracting the current signal based on the traditional satellite tracking loop was studied and verified by many field experiments. During the target movement, the FSR signal produces an appropriate Doppler frequency shift [21]. This work provided a simplified model of the received signal and analyzed its Doppler characteristics in [22]; however, none of these works has focused on extracting the characteristics from satellite communication waveforms for target sensing; therefore, it is of great significance to study the problem of aerial target sensing in the case of forward scatter.

In this paper, a novel satellite communication waveforms-based aerial target sensing method is proposed, and the main contributions of this paper are as follows:

- In order to purify the signal, a zero-notch filter is used to separate the direct wave signal. In addition, the multipath interference is suppressed based on the reversibility of the linear canonical transformation and the suppression effect of Gaussian noise;
- The linear canonical transformation is used to process the signal after interference suppression, and the detection statistic is extracted to sense the aerial target;
- Through the analysis of the forward scatter signal and the characteristics of the linear canonical transformation algorithm, the linear canonical transformation and the matched filter algorithm are combined to estimate the target parameters.

The remainder of this paper is organized as follows. In Section 2, the system model used in this paper is presented. The suppression of multipath interference is described in Section 3. Detection statistics and the detector design are proposed in Section 4. In Section 5, the performance of target detection is analyzed. Two methods of parameter estimation are proposed in Section 6. In Section 7, the performance of parameter estimation is analyzed. Section 8 shows the numerical results to verify the classification performance. Finally, Section 9 concludes the paper.

2. System Model

The GPS waveforms-based forward scatter system is shown in Figure 1. Since the bistatic angle is close to 180°, the signals received by the receiving antenna include direct wave signals, forward scatter signals, multipath interference, and noise. Thus, it requires direct wave suppression and multipath interference suppression for target sensing and target parameter estimation.

The geometry of the forward scatter system is shown in Figure 2. In Figure 2, multipath refers to the propagation of radio signals from the transmitting antenna to the receiving antenna through multiple paths. The scattering of radio waves by the atmosphere, the reflection and refraction of radio waves by the ionosphere, and the reflection of radio waves by surface objects, such as mountains and buildings, will all cause multipath propagation. The system uses GPS as the illuminator, and the receiver is located at the O point of the coordinate system. It is assumed that the satellite transmitter is located on the xOz plane, and that the target moves at a speed v and height H in a plane parallel to the ground. θ_{SV} denotes the angle between the baseline and the z axis, and θ_v represents the projection angle between the target trajectory on the ground and the axis. Assuming that the target crosses the baseline, or is near the baseline, R_D, R_T, R_R are the distances from the transmitter to

the receiver, from the transmitter to the target, from the receiver to the target, respectively. θ represents the angle between R_D and R_R.

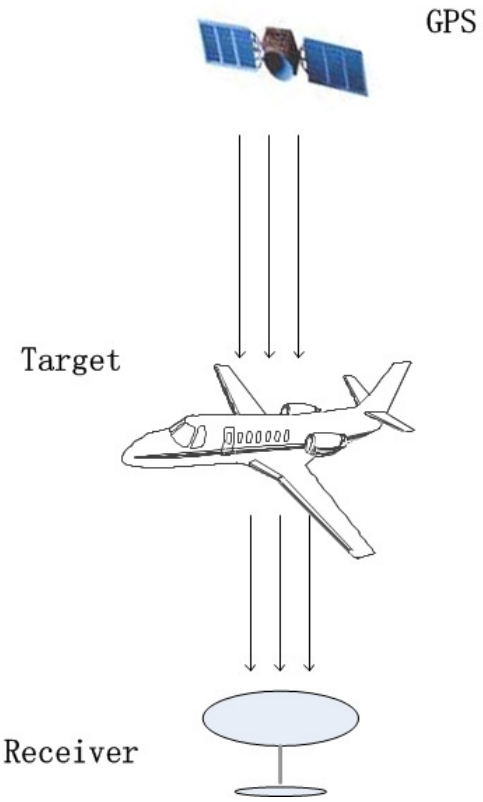

Figure 1. GPS waveforms-based forward scatter system model.

Compared with conventional radar, the main difference of FSR is its scattering characteristics. In the FSR configuration, the received signal includes the direct wave signal $s_d(t)$ from the transmitter, the forward scatter signal $s_t(t)$ due to the presence of the aerial target, the multipath interference and noise; therefore, the signal received by the receiver can be described as

$$\begin{aligned} x(t) &= A_d s(t-\tau_d(t)) + A_T s(t-\tau_t(t)) e^{j\varphi_\sigma} + \sum_{j=1}^{H} \omega_j s\big(t-\tau_{\eta j}(t)\big) + n(t) \\ &= \sqrt{P_d} C^k(t-\tau_d(t)) D^k(t-\tau_d(t)) e^{2\pi f_0(t-\tau_d)} \\ &+ \sqrt{P_t} C^k(t-\tau_t(t)) D^k(t-\tau_t(t)) e^{2\pi f_0(t-\tau_t)} e^{j\varphi_\sigma} \\ &+ \sum_{j=1}^{H} \omega_j s\big(t-\tau_{\eta j}(t)\big) + n(t), \end{aligned} \tag{1}$$

where A_d denotes the amplitude of the direct wave signal, A_T represents the amplitude of the forward scatter signal, φ_σ is the scatter phase, and H stands for the order of the multipath channel. ω_j is the amplitude of the direct wave signal after passing through the jth multipath, $\tau_{\eta j}(t)$ represents the delay of the direct wave signal after passing through the jth multipath, and $n(t)$ is stationary Gaussian white noise with mean zero. C^k is the C/A code of the satellite signal and D^k is the satellite nanvigation data. P_d denotes the power of the direct wave signal and P_t represents the power of the forward scatter signal. In addition, $\tau_d(t)$ and $\tau_t(t)$ indicate delays in the direct and target channels as

$$\tau_d(t) = \frac{R_D(t)}{c}, \tag{2}$$

$$\tau_t(t) = \frac{R_T(t) + R_R(t)}{c}, \tag{3}$$

where c denotes the velocity of light.

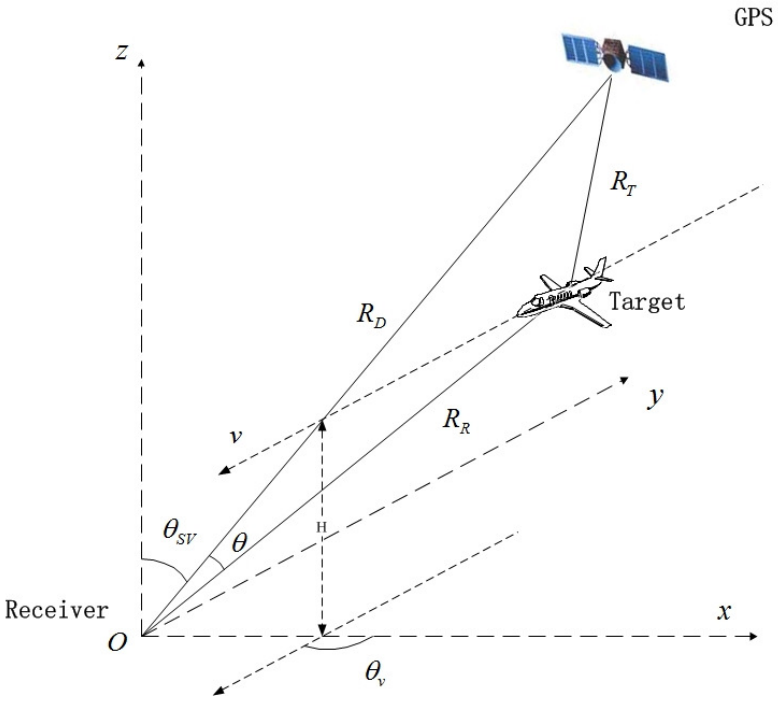

Figure 2. Geometric model of forward scatter system.

As the target moves, the scattered signal $s_t(t)$ exhibits a Doppler change, and its amplitude modulation is specified by the forward scatter mode and the propagation loss. In the forward scatter scenario, it is assumed that the arrival time of the direct wave and forward scatter signal are nearly the same. In this case, there is no distance offset between the two signals, so the effect of the delay difference in the C/A code and the navigation code can be ignored; therefore, the received signal can be rewritten as

$$\begin{aligned} x(t) = \sum_{j=1}^{H} \omega_j s\left(t-\tau_{\eta j}(t)\right) + n(t) + C^k(t-\tau_d(t)) D^k(t-\tau_t(t)) \\ \times \left(\sqrt{P_d} e^{2\pi f_0(t-\tau_d(t))} + \sqrt{P_t} e^{2\pi f_0(t-\tau_t(t))} e^{j\varphi_\sigma}\right). \end{aligned} \tag{4}$$

Since there is no reference channel for the FSR system, it is necessary to perform preprocessing on the received signal before radar processing. The preprocessing flow chart is shown in Figure 3 [23]. In the tracking loop, the code phase and the carrier spectrum are accurately estimated by the code tracking loop and the carrier tracking loop, respectively. I/Q demodulation is often used to realize the tracking loop. According to [24], code correlation and symbol elimination are performed on the received signal after the down conversion, and the correlation result after signal processing can be obtained as

$$x_{r1}(t) = G_d + G_T A_T e^{2\pi f_0(\tau_d(t)-\tau_t(t)-\varphi_\sigma)} + \sum_{j=1}^{H} \omega_{\eta j} e^{2\pi f_0\left(\tau_{\eta j}(t)-\tau_d(t)\right)} + n'(t), \tag{5}$$

where G_d and G_T are the code correlation gain of the direct wave and target echo, respectively. $\omega_{\eta j}$ stands for the amplitude of the jth multipath interference, and $n'(t)$ is the Gaussian white noise with mean zero. The output results after processing are shown in Figures 4 and 5.

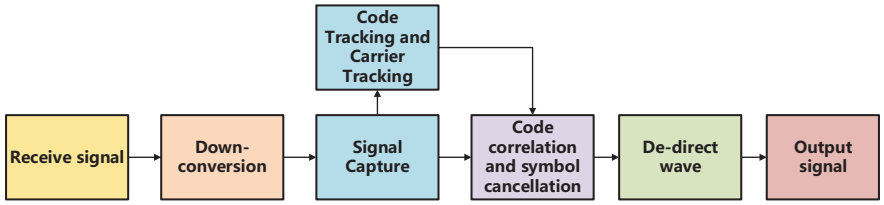

Figure 3. Flow chart of forward scatter signal preprocessing.

Notch filter refers to a filter that can rapidly attenuate the signal at a certain frequency to remove the signal at this frequency. It belongs to a bandstop filter, and its stopband is very narrow. Due to the target motion, the target echo signal presents Doppler change. In the forward scattering scenario, it can be assumed that the arrival time of direct wave and target echo to the receiver is basically the same, and that there is no distance deviation between the two signals. Then the output of the code correlation processing of the two signals can be considered to be coherent, and the amplitude of the code correlation results can be obtained. According to [24], since each processing cycle is within a few milliseconds of single-chirp integration time, we can regard the frequency of direct signal and echo signal as constants. For direct signals, this assumption is widely used in traditional navigation satellite signal processing; therefore, the suppression of direct wave signal can be completed by a notch filter. In this case, the received signal can be given by

$$x_r(t) = G_T A_T e^{2\pi f_0(\tau_d - \tau_t - \varphi_\sigma)} + \sum_{j=1}^{H} \omega_{\eta j} e^{2\pi f_0(\tau_{\eta j} - \tau_d)} + n'(t). \tag{6}$$

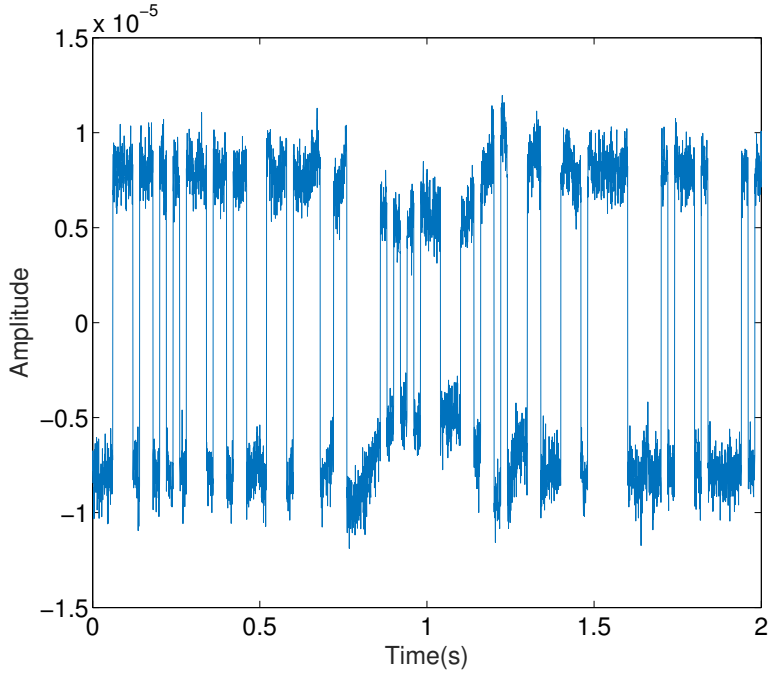

Figure 4. Output signal after code correlation.

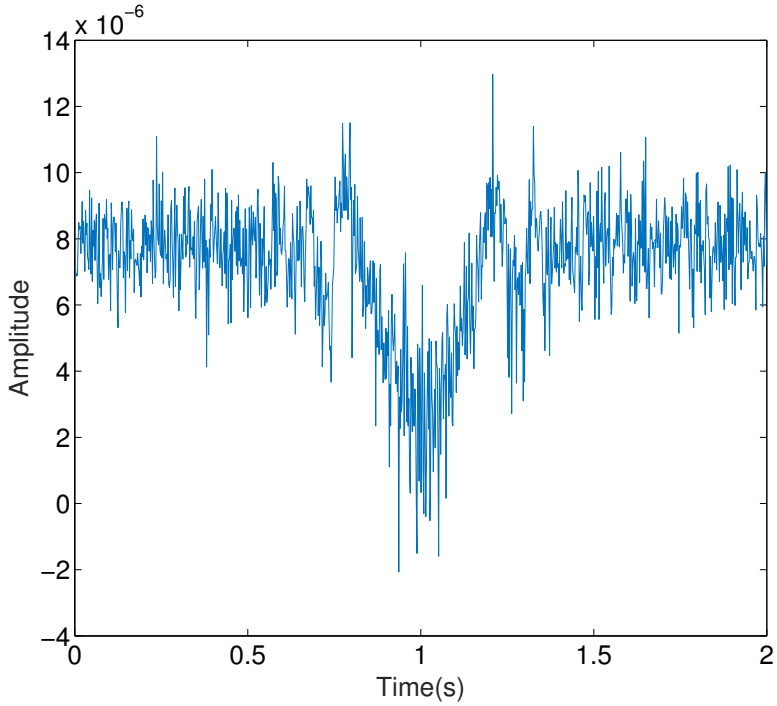

Figure 5. Output signal after symbol elimination.

3. Multipath Interference Suppression

Since the received signal is inevitably affected by the direct wave and multipath interference, the power of the direct wave and multipath interference is higher than the power of the echo signal containing the target. This will affect the sensing. Thus it is necessary to suppress the direct wave and multipath interference.

Linear canonical transform (LCT) is a generalized form of Fourier transform, which has multiple free parameters. Compared with the traditional Fourier transform, it has great flexibility. The traditional method of separating signal and noise is only carried out in either the time domain or the frequency domain, but it is difficult to obtain good filtering and interference separation effect in time domain or frequency domain if there is strong time-frequency coupling between signal components and between signal and noise. In this case, the LCT provides a more suitable filtering and interference separation scheme in another transform domains. For the problem of multipath interference in the receiving channel, using the reversibility of the linear canonical transform and its suppression of Gaussian noise, the Gaussian noise and multipath interference in the channel can be removed by the rectangular window function in its linear regular domain. Thus, the signal after noise suppression is obtained through inverse linear regular transformation. In contrast, Fourier transform can only remove noise and cannot effectively suppress multipath interference; therefore, we choose the linear canonical transform with better filtering and interference separation performance to process the signal.

The signal distribution before the multipath interference suppression in the LCT domain is shown in Figure 6. In Figure 6, u represents the LCT domain. Fourier transform and fractional Fourier transform are special forms of LCT, so LCT domain can be regarded as the unity of time domain, frequency domain, and fractional Fourier domain, and contains the information of signal in time domain and frequency domain. Since most of the energy of the echo signal is concentrated in a narrow band centered at the peak point of the linear canonical transform domain, the Gaussian noise does not have good energy concentration in the LCT domain. It can also be seen that the energy distribution of multipath interference is on both sides of the LCT domain; therefore, the peak point can be used as the center of the rectangular window function to filter out the noise and interference.

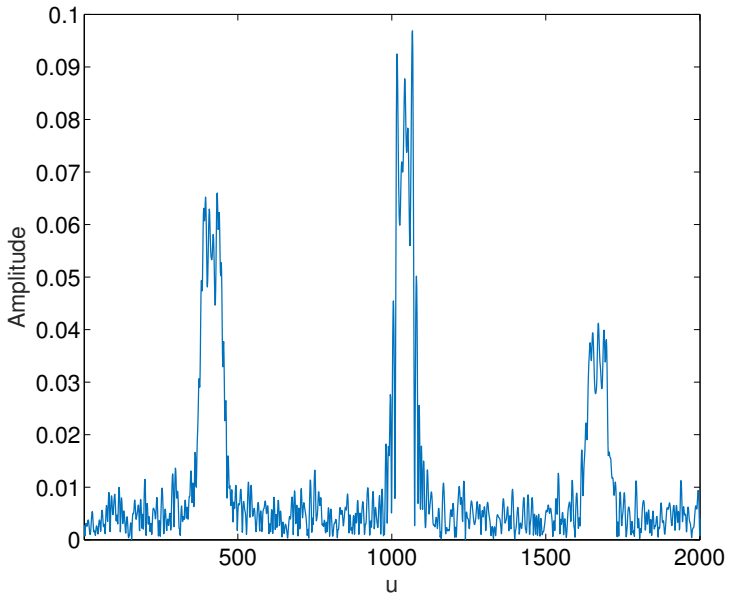

Figure 6. Linear canonical transform of the signal before multipath interference suppression.

The steps to design the bandwidth of the rectangular window function are summarized in Algorithm 1.

According to the above analysis, the window function can be constructed to extract the echo signal. The rectangular window function in the linear canonical domain can be expressed as

$$\ell[f(t)](u) = \begin{cases} 1 & u \in [a, b], \\ 0 & else. \end{cases} \tag{7}$$

By applying the reversibility of the LCT algorithm to transform the separated signal, the suppression of direct wave and multipath interference can be achieved. The suppressed signal is subject to LCT again, and the suppression effect is determined by observing whether there is a corresponding peak in the LCT domain. The effect of interference suppression on the signal is shown in Figure 7. From Figure 7, we can see that the multipath interference have been well suppressed.

Algorithm 1 Rectangular window function bandwidth design

1: Perform LCT on the signal to obtain the LC spectrum of the signal $P_L(w)$;
2: Perform least squares polynomial fitting to obtain a smooth power spectrum curve;
3: Derivative the smoothness power spectrum curve, and extract the positions of the maximum and minimum points of the slope derivative value near the center point of the LC domain from a and b, respectively. Further, use the difference $|b - a|$ as the bandwidth estimation;
4: Design the number of cycles and repeat the above operation to obtain the statistical average.

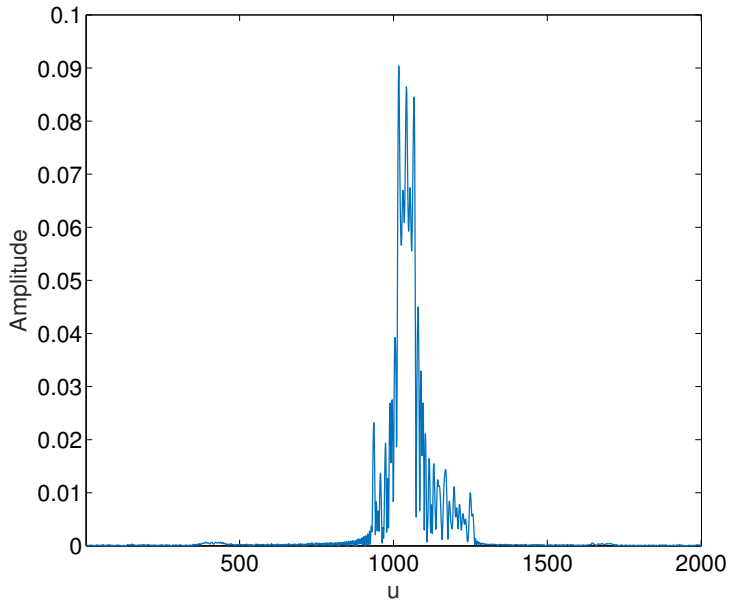

Figure 7. Linear canonical transform of the signal after multipath interference suppression.

4. Aerial Target Passive Sensing Based on Linear Canonical Transform

Based on the above analysis, the amplitude and phase of the received signal are mainly reflected in the shadow occlusion effect and the approximate chirp Doppler phenomenon. Using these characteristics, and considering the outstanding performance of LCT in chirp signal processing, this paper proposes the aerial target sensing based on LCT.

4.1. Signal Delay Analysis

One sees that the change in the time delay change of the signal makes the echo signal equivalent to a frequency-modulated signal. Since the satellite is far away from the ground, it is assumed that the target echo signal is parallel to the direct incident wave arriving at the receiver, or assumed a plane wave. Assuming that the time is zero when the target traverses the xOz plane, the flying height of the target is H, and the distance between the projection on the ground and the receiver is x_0, the position of the target trajectory can be expressed as

$$\begin{cases} x_{SV}(t) = L\sin\theta_{SV}, \\ y_{SV}(t) = 0, \\ z_{SV}(t) = L\cos\theta_{SV}, \end{cases} \tag{8}$$

and the trajectory of the satellite is

$$\begin{cases} x(t) = vt\cos\theta_v + x_0, \\ y(t) = vt\sin\theta_v, \\ z(t) = H, \end{cases} \tag{9}$$

where L denotes the baseline length at $t = 0$. Under the assumption of plane waves, $R_D = R_T + R_R\cos\theta$; therefore, the delay difference can be written as

$$\Delta\tau(t) = \frac{R_T + R_R - R_D}{c} = \frac{R_R - R_R\cos\theta}{c}. \tag{10}$$

Applying the Pythagorean theorem and substituting the expressions of target trajectory and satellite trajectory into (10), we can obtain

$$\begin{aligned}\Delta\tau(t) &= \frac{R_R}{c} - \frac{[x(t), y(t), z(t)][x_{SV}(t), y_{SV}(t), z_{SV}(t)]^T}{c\sqrt{x_{SV}^2(t) + y_{SV}^2(t) + z_{SV}^2(t)}} \\ &= \frac{R_R}{c} - \frac{vt\cos\theta_v \sin\theta_{SV} + x_0 \sin\theta_{SV} + H\cos\theta_{SV}}{c},\end{aligned} \tag{11}$$

where R_R can be expressed as

$$\begin{aligned}R_R &= \sqrt{(vt\cos\theta_v + x_0)^2 + (vt\sin\theta_v)^2 + H^2} \\ &= \sqrt{v^2t^2 + 2vtx_0\cos\theta_v + {x_0}^2 + H^2}.\end{aligned} \tag{12}$$

Taking the third-order Maclaurin of ${x_0}^2 + H^2$ about $v^2t^2 + 2vtx_0\cos\theta_v$, we can obtain

$$\begin{aligned}R_R &\approx \sqrt{{x_0}^2 + H^2} + \frac{v^2t^2 + 2vtx_0\cos\theta_v}{2\sqrt{{x_0}^2 + H^2}} - \frac{\left(v^2t^2 + 2vtx_0\cos\theta_v\right)^2}{8({x_0}^2 + H^2)\sqrt{{x_0}^2 + H^2}} \\ &= \sqrt{{x_0}^2 + H^2} - \frac{v^4t^4 + 4v^3t^3x_0\cos\theta_v}{8({x_0}^2 + H^2)\sqrt{{x_0}^2 + H^2}} \\ &+ \frac{v^2t^2\left(1 - \frac{x_0^2\cos^2\theta_v}{{x_0}^2 + H^2}\right) + 2vtx_0\cos\theta_v}{2\sqrt{{x_0}^2 + H^2}}.\end{aligned} \tag{13}$$

By omitting the third term and the fourth term of t, (13) can be rewritten as

$$R_R \approx \sqrt{{x_0}^2 + H^2} + \frac{v^2t^2\left(1 - \frac{x_0^2\cos^2\theta_v}{{x_0}^2 + H^2}\right) + 2vtx_0\cos\theta_v}{2\sqrt{{x_0}^2 + H^2}}. \tag{14}$$

Substituting (14) into (11), the available delay difference is expressed as

$$\begin{aligned}\Delta\tau(t) = &\frac{\sqrt{{x_0}^2 + H^2} - x_0\sin\theta_{SV} - H\cos\theta_{SV}}{c} + \frac{v^2t^2\left(1 - \frac{x_0^2\cos^2\theta_v}{{x_0}^2 + H^2}\right)}{2c\sqrt{{x_0}^2 + H^2}} \\ &+ \frac{vt}{c}\left(\frac{x_0\cos\theta_v}{\sqrt{{x_0}^2 + H^2}} - \cos\theta_v\sin\theta_{SV}\right).\end{aligned} \tag{15}$$

Considering the case of crossing the baseline at the moment of $t = 0$ and substituting $x_0 = H\tan\theta_{SV}$ into (15), we can obtain

$$\Delta\tau(t) = \frac{v^2t^2\cos\theta_{SV}\left(1 - \cos^2\theta_v\sin^2\theta_{SV}\right)}{2cH}. \tag{16}$$

Based on (15), the time delay difference in the case of forward scatter can be calculated. The exact expression (11) and the approximate expression (15) are used to calculate the time delay difference, and the simulation results are shown in Figures 8 and 9. It can be seen that the curves can be described by different equations. It also shows that the above simplification is effective, which can provide theoretical support for the target sensing and target parameter estimation. From Figure 8, we can see that the influence of the speed direction angle on the delay difference is very small. Assuming that the target does not cross the baseline and the horizontal distance from the baseline when crossing the xOz plane is 50 m, the simulation is shown in Figure 9. It can be seen from Figure 9 that the

delay difference in both cases are very close, and hence this paper only considers the case when the target crosses the baseline.

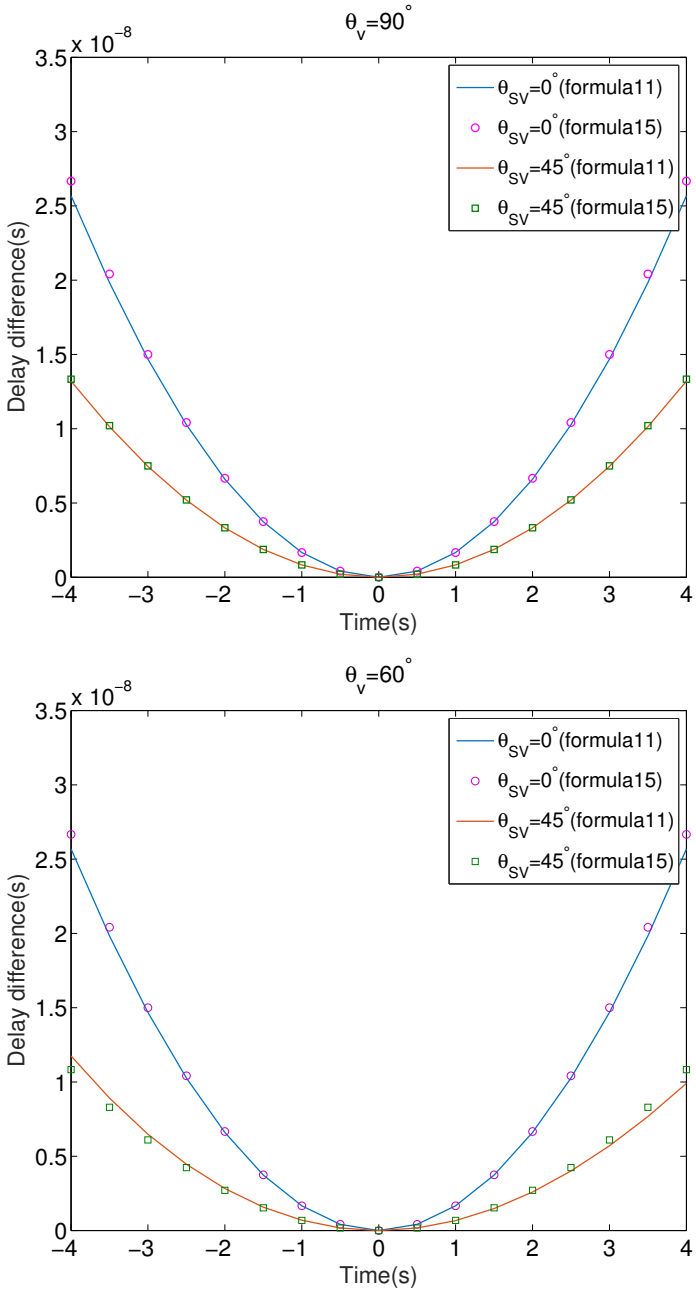

Figure 8. Different delay when the target crosses the baseline.

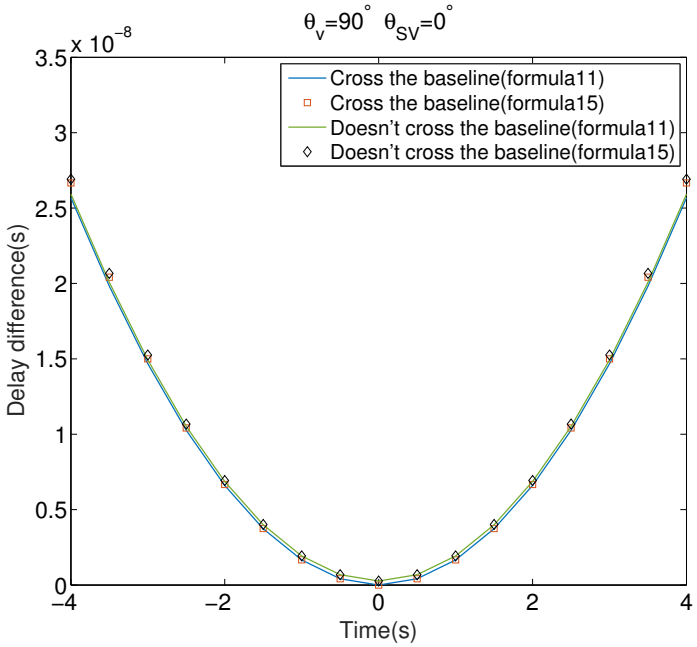

Figure 9. Different delay when the target does not cross the baseline.

4.2. Target Sensing Statistics

The LCT of the signal after the suppression of direct wave and multipath interference is expressed as [25]

$$L(u) = \frac{1}{\sqrt{j2\pi b}} \int_{-\frac{T}{2}}^{\frac{T}{2}} f(t) e^{j\frac{a}{2b}t^2 - j\frac{u}{b}t + j\frac{du^2}{2b}} dt. \tag{17}$$

After discretization, this becomes

$$L(u) = \frac{1}{\sqrt{j2\pi b}} \sum_{n=0}^{N-1} f(nT_s) e^{j\frac{a}{2b}(nT_s)^2 - j\frac{u}{b}nT_s + j\frac{du^2}{2b}}, \tag{18}$$

where T stands for the signal duration, T_s denotes the sampling period, $T_s = 1/f_s$, N is the number of sampling points $N{=}T_s \times f_s$. The target sensing statistic l is constructed as

$$l = |L(u)|. \tag{19}$$

4.3. Target Detection

The detector is binary, where H_1 indicates that the received signal, $x(t)$ contains an echo signal, and H_0 indicates that the received signal does not contain an echo signal, as

$$\begin{cases} H_0 : x(t) = v(t), \\ H_1 : x(t) = A_T s_r(t) + w(t). \end{cases} \tag{20}$$

Based on the above binary assumption, the binary detector is

$$|l| \underset{H_0}{\overset{H_1}{\gtrless}} T_d, \tag{21}$$

where T_d represents the detection threshold. The decision output u is

$$u = \begin{cases} 1 & |l| > T_d, \\ 0 & else. \end{cases} \tag{22}$$

5. Detection Performance Analysis

Assuming that both the real and imaginary parts of the Gaussian noise follow $N\left(0,\sigma_n^2\right)$, one has

$$\begin{aligned} L(u) &= \int_{-\frac{T}{2}}^{\frac{T}{2}} x(t)K_A(u,t)dt \\ &= \mathrm{Re}\left\{\int_{-\frac{T}{2}}^{\frac{T}{2}} x(t)K_A(u,t)dt\right\} + \mathrm{Im}\left\{\int_{-\frac{T}{2}}^{\frac{T}{2}} \mathrm{x(t)K_A(u,t)dt}\right\} \\ &= l_R + l_I. \end{aligned} \tag{23}$$

Lemma 1. *The distribution of the detection based on LCT under H_1 is*

$$(l|H_1) \sim CN\left(\int_{-\frac{T}{2}}^{\frac{T}{2}} A_T s_r(t)K_A(u,t)dt, \sigma_{nn}^2\right), \tag{24}$$

and the distribution of the detection based on LCT under H_0 is

$$(l|H_0) \sim CN\left(0,\sigma_{nn}^2\right), \tag{25}$$

where $CN(\cdot)$ represents the complex Gaussian process.

Proof. See Appendix A. □

From the above analysis, the detection probability P_D is

$$\begin{aligned} P_D &= \int_{\lambda}^{+\infty} p(l|H_1)dl \\ &= \int_{\lambda}^{+\infty} \frac{2l}{\sigma_{nn}^2} \exp\left(-\frac{l^2 + \left|\int_{-\frac{T}{2}}^{\frac{T}{2}} A_T s_r(t)K_A(u,t)dt\right|^2}{\sigma_{nn}^2}\right) \\ &\times I_0\left(\frac{2l\cdot\left|\int_{-\frac{T}{2}}^{\frac{T}{2}} A_T s_r(t)K_A(u,t)dt\right|}{\sigma_{nn}^2}\right)dl \\ &= Q\left(\sqrt{\frac{2\left|\int_{-\frac{T}{2}}^{\frac{T}{2}} A_T s_r(t)K_A(u,t)dt\right|^2}{\sigma_{nn}^2}}, \sqrt{2\ln\frac{1}{P_{fa}}}\right), \end{aligned} \tag{26}$$

where $p(l|H_1)$ represents the probability density function of $(l|H_1)$ and $Q(\cdot,\cdot)$ denotes the Marcum Q function [26]. The false alarm probability P_{fa} is

$$\begin{aligned} P_{fa} &= \int_{\lambda}^{+\infty} p(l|H_0)dl \\ &= \int_{\lambda}^{+\infty} \left(2l\Big/\sigma_{nn}^2\right)\exp\left(l^2\Big/\sigma_{nn}^2\right)dl \\ &= \exp\left(\lambda^2\Big/\sigma_{nn}^2\right), \end{aligned} \tag{27}$$

where $p(l|H_0)$ represents the probability density function of $(l|H_0)$. The threshold λ of false alarm probability detection can be expressed as

$$\lambda = \sqrt{-\sigma_{nn}^2 \ln P_{fa}}. \tag{28}$$

6. Aerial Target Parameter Estimation

6.1. Parameter Estimation Based on LCT+MF

When the target gradually approaches and then moves away from the baseline at a constant speed, the sum of the distances from the transmitter to the target and from the target to the receiver changes. Linear frequency modulation (LFM) signal increases the transmission bandwidth of the signal by modulating the carrier frequency, and realizes pulse compression at reception. The forward scatter system does not have a reference signal, but when the moving speed of the target is slow, the Doppler frequency shift is small and the frequency change is slow. At this time, the echo signal can be approximated as a chirp signal with frequency change. Based on this, the feature function is constructed, and the speed and flight altitude can be estimated through the matched filtering (MF). The target parameter estimation system diagram based on LCT+MF is shown in Figure 10.

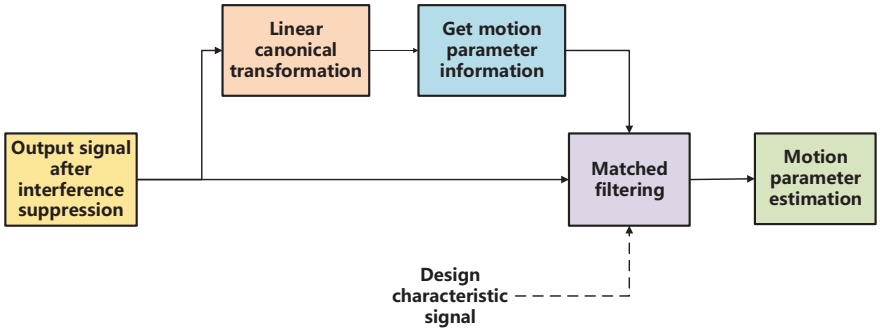

Figure 10. Target parameter estimation system diagram based on LCT+MF.

The LCT-based method can effectively separate the signal and the interference, thereby reduce the influence of interference and improve the accuracy of parameter estimation. By designing the four parameters (a, b, d, u) in the LCT domain, the spectral peak information is obtained in the LCT domain. The corresponding parameters at the spectral peak include the target parameter information $H_{\max}, v_{\max}, \theta_{v_{\max}}$ of the moving target. One has

$$|l| \underset{H_0}{\overset{H_1}{\gtrless}} T_d. \tag{29}$$

The relationship between the target parameters can be estimated according to the characteristics of the parameter $\left(\hat{a}, \hat{b}, \hat{d}, \hat{u}\right)$ at the peak and the forward scattered signal as

$$|l| \underset{H_0}{\overset{H_1}{\gtrless}} T_d. \tag{30}$$

The coordinates (a, b, d, u) corresponding to the peak can be effectively extracted using the following peak extraction methods summarized in Algorithm 2.

Algorithm 2 Extraction of spectrum peak in LCT domain.

1: The LCT $L(u)$ contains four parameters. If two-dimensional spectrum peak is searched, and the parameter values b and d of LCT domain are fixed firstly;
2: Determine $\hat{b}$ and $\hat{d}$, and a two-dimensional peak search on $a \times u$ on the (a, u) plane;
3: For different values of a perform spectral peak search on the one-dimensional plane, and take the corresponding parameter $\hat{a}$ at the maximum peak.

The target parameters are related through $v^2 \cos\theta_{SV}\left(1-\cos^2\theta_v \sin^2\theta_{SV}\right) = -\frac{\hat{a}}{2\hat{b}}\frac{2cH}{j2\pi f_c}$. The steps of parameter estimation based on LCT+MF are as follows:

Step 1: Construct the feature function as

$$f(t) = a_F e^{j2\pi f_c q(v,H)t^2}, \tag{31}$$

where a_F represents the amplitude of the characteristic function, f_c stands for the carrier frequency, and $q(v, H)$ is a function of the parameters v and H with $q(v,H) = \frac{v^2 \cos\theta_{SV}\left(1-\cos^2\theta_v \sin^2\theta_{SV}\right)}{2cH}$.

Step 2: Perform matching filtering as [27]

$$S_{out}(v_m, H_m) = \int_{-\frac{T}{2}}^{\frac{T}{2}} y^*(t) \cdot f(t) dt, \tag{32}$$

where T is the observation time, $*$ represents the conjugate operation, $S_{out}(v_m, H_m)$ stand for the output result, and $y(t)$ is the received signal after interference suppression. Substituting the known relationship between v and H into (32), we can obtain

$$S_{out}(H_m) = \int_{-\frac{T}{2}}^{\frac{T}{2}} y^*(t) \cdot f(t) dt. \tag{33}$$

Step 3: To obtain more accurate estimates. In this process, Δv and ΔH are shortened to obtain a more accurate estimate according to the estimated v and H values.

6.2. Parameter Estimation Based on MF+LCT

Since the LCT can achieve effective separation of signal and noise by reducing the influence of noise on matched filtering, the LCT process is performed on the matched filtering. The target parameter estimation system diagram based on MF+LCT is shown in Figure 11.

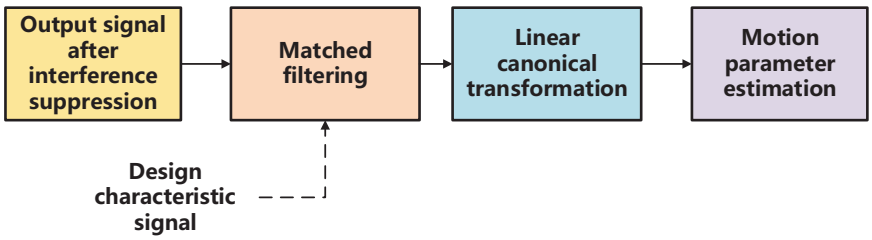

Figure 11. Target parameter estimation system diagram based on MF+LCT.

After matching filtering, the signal is transformed into the LCT domain, and the target parameters are estimated by searching for the peak value. The steps of parameter estimation based on MF+LCT are as follows:

Step 1: Construct the feature function as

$$f(t) = a_F e^{j2\pi f_c q(v,H)t^2}, \tag{34}$$

where a_F represents the amplitude of the characteristic function, f_c is the carrier frequency, and $q(v, H)$ stands for a function about the parameters v and H with $q(v, H) = \frac{v^2 \cos\theta_{SV}\left(1-\cos^2\theta_v \sin^2\theta_{SV}\right)}{2cH}$.

Step 2: Perfom matching filtering and transform it to LCT domain as

$$SL_{out}(v_m, H_m) = \frac{1}{\sqrt{j2\pi b}} \int_{-\frac{T}{2}}^{\frac{T}{2}} y^*(t) \cdot f(t) e^{j\frac{a}{2b}t^2 - j\frac{u}{b}t + j\frac{du^2}{2b}} dt, \tag{35}$$

where T represents the observation time, $*$ denotes the conjugate operation, $S_{out}(v_m, H_m)$ is the output result, and $y(t)$ stands for the received signal after interference suppression.

7. CRLBs of Target Parameter Estimators

Assume that $y(t)$ is the signal after interference suppression and contains only echo signals and noise, and thus $y(t)$ can be rewritten as:

$$y(t) = a_{Tt} e^{j2\pi f_0(\tau_d - \tau_t)} + m(t), \tag{36}$$

where a_{Tt} represents the amplitude of the echo signal, $m(t)$ is Gaussian noise with mean zero and $\Delta\tau = \tau_t - \tau_d$. The power spectral density of the noise is

$$E\left[m(t)m\left(t'\right)\right] = 0, \tag{37}$$

$$E\left[m(t)m^*\left(t'\right)\right] = N_0\delta\left(t - t'\right). \tag{38}$$

The vector form of the estimation speed and the estimation height can be expressed as

$$\theta = [v, H]. \tag{39}$$

The probability density function (PDF) of the echo signal can be expressed as [28,29]:

$$p(y;\theta) = K\exp\left\{-\frac{1}{N_0}\int_{-\infty}^{+\infty}\left|y(t) - a_{Tt}e^{-j2\pi f_0\Delta\tau}\right|^2 dt\right\}. \tag{40}$$

Accordingly, the natural logarithmic of PDF is given by

$$\ln p(y;\theta) = -\frac{1}{N_0}\int_{-\infty}^{+\infty}\left|y(t) - a_{Tt}e^{-j2\pi f_0\Delta\tau}\right|^2 dt + \ln K. \tag{41}$$

By differentiating the logarithmic PDF, one has

$$\frac{\partial \ln p(y;\theta)}{\partial v} = -\frac{2}{N_0}\int_{-\infty}^{+\infty} m^*(t) \times \left(-\frac{\partial a_{Tt}}{\partial v} + j2\pi f_0 a_{Tt}\frac{\partial \Delta\tau}{\partial v}\right) e^{-j2\pi f_0\Delta\tau} dt, \tag{42}$$

and

$$\frac{\partial \ln p(y;\theta)}{\partial H} = -\frac{2}{N_0}\int_{-\infty}^{+\infty} m^*(t) \times \left(-\frac{\partial a_{Tt}}{\partial H} + j2\pi f_0 a_{Tt}\frac{\partial \Delta\tau}{\partial H}\right) e^{-j2\pi f_0\Delta\tau} dt. \tag{43}$$

According to the parameter estimation theory, the CRLB is

$$\mathrm{var}(\theta_i) \geq \left[I^{-1}(\theta)\right]_{ii}. \tag{44}$$

where $\left[I^{-1}(\theta)\right]_{ii}$ is the (i, i)-th element of the inverse matrix of the FIM matrix, and the FIM matrix is

$$[I(\theta)]_{ij} = I_{ij} = E\left[\frac{\partial \ln P(y;\theta)}{\partial \theta_i}\frac{\partial \ln P(y;\theta)}{\partial \theta_j}\right]. \tag{45}$$

Define the following variables

$$G_{\mathrm{ij}} = \int_{-\infty}^{+\infty} \left(\frac{\partial a_{Tt}}{\partial \theta_i}\right)^* \left(\frac{\partial a_{Tt}}{\partial \theta_j}\right) dt, \tag{46}$$

$$Q_{\mathrm{ij}} = \int_{-\infty}^{+\infty} a_{Tt}^2 \left(\frac{\partial \Delta\tau}{\partial \theta_i}\right)^* \left(\frac{\partial \Delta\tau}{\partial \theta_j}\right) dt, \tag{47}$$

and

$$R = \int_{-\infty}^{+\infty} a_{Tt} \left(\left(\frac{\partial a_{Tt}}{\partial \theta_j}\right)^* \frac{\partial \Delta\tau}{\partial \theta_i} + \left(\frac{\partial \Delta\tau}{\partial \theta_j}\right)^* \frac{\partial a_{Tt}}{\partial \theta_i} \right) dt. \tag{48}$$

The elements of the available FIM matrix are

$$\begin{aligned} I_{ii} &= -\frac{2}{N_0} \int_{-\infty}^{+\infty} \left(\left(\frac{\partial a_{Tt}}{\partial \theta_i}\right)^2 + (2\pi f_0 a_{Tt})^2 \left(\frac{\partial \Delta\tau}{\partial \theta_i}\right)^2 \right) dt \\ &= -\frac{2}{N_0} \left(G_{ii} + (2\pi f_0)^2 Q_{ii} \right), \end{aligned} \tag{49}$$

$$\begin{aligned} & I_{ij,i\neq j} = I_{ji,i\neq j} \\ &= -\frac{2}{N_0} \int_{-\infty}^{+\infty} \left(\frac{\partial a_{Tt}}{\partial \theta_j}\right)^* \left(\frac{\partial a_{Tt}}{\partial \theta_i}\right) + (2\pi f_0 a_{Tt})^2 \left(\frac{\partial \Delta\tau}{\partial \theta_j}\right)^* \left(\frac{\partial \Delta\tau}{\partial \theta_i}\right) \\ &+ j2\pi f_0 a_{Tt} \left(\left(\frac{\partial a_{Tt}}{\partial \theta_j}\right)^* \frac{\partial \Delta\tau}{\partial \theta_i} + \left(\frac{\partial \Delta\tau}{\partial \theta_j}\right)^* \frac{\partial a_{Tt}}{\partial \theta_i} \right) dt \\ &= -\frac{2}{N_0} \left(G_{ij} + (2\pi f_0)^2 Q_{ij} + j2\pi f_0 R \right). \end{aligned} \tag{50}$$

Then, the FIM can be expressed in (51).

$$\begin{aligned} I(\theta) &= \frac{-2}{N_0} \begin{bmatrix} G_{11} + (2\pi f_0)^2 Q_{11} & G_{12} + (2\pi f_0)^2 Q_{12} + j2\pi f_0 R \\ G_{12} + (2\pi f_0)^2 Q_{12} + j2\pi f_0 R & G_{22} + (2\pi f_0)^2 Q_{22} \end{bmatrix} \\ &= -\frac{2}{N_0} \begin{bmatrix} A & B \\ B & C \end{bmatrix}, \end{aligned} \tag{51}$$

The inverse of the FIM matrix, and normalized Cramér–Rao lower bound (NCRLB) of the estimation speed and height can be expressed as

$$Var(\hat{v})_{NCRLB} = \frac{N_0 C}{B^2 - AC}, \tag{52}$$

and

$$Var\left(\hat{H}\right)_{NCRLB} = \frac{N_0 A}{B^2 - AC}. \tag{53}$$

8. Numerical Results and Discussion

In order to evaluate the performance of the proposed method, the GPS satellite communication waveforms are used. The sensing performance is determined by [30,31]

$$\delta_H = \frac{N_r}{N} \times 100\%, \tag{54}$$

where δ_H represents the detection accuracy, N_r and N are the numbers of correct detections and the total number of detections, respectively.

In the simulation, we adopt the GSM TU 6 channel model. Using this multipath fading model, the following experiments examine the performance of the proposed algorithm for target echo signal detection.

In order to evaluate the influence of sampling points on the sensing performance, the parameters are set as follows: the sampling frequency is $f_s = 10.23$ MHz , the false alarm probability is $P_{fa} = 10^{-4}$, the GPS direct wave power is $P_d = -100$ dBm, the symbol rate is $f_{Gb} = 1.023$ MHz, the carrier frequency is $f_c = 1.57$ GHz, the aerial target altitude is 10 km, the flight speed is 100 m/s, the average power of the echo signal is $P_r = -135$ dBm; 2000 Monte Carlo simulations are used.

It can be seen from Figure 12 that the target sensing performance improves as the number of sampling points increases. This is because the increase in the number of sampling points will increase the cumulative number of points in the time domain, resulting in the enhancement of the peak height in the corresponding LCT domain, thus improving the sensing performance. Although the number of sampling points is an important factor, the limited sensing range in the case of forward scatter prevents sampling points from increasing indefinitely, and the sampling points should be set reasonably. When the number of sampling points is 5×10^6, the sensing performance reaches 100% with SNR = -31 dB. When the number of sampling points is 10^7, the sensing performance can reach 100% with SNR = -36 dB, and when the number of sampling points is 2×10^7, the sensing performance can reach 100% with SNR = -37 dB. At the same time, it can be seen that under the same number of sampling points, as the signal-to-noise ratio increases, the detection effect is better. The actual simulation performance is basically consistent with the theoretical derivation, which verifies the effectiveness of the proposed method.

In order to evaluate the target sensing performance of forward scatter echo signal for different false alarm probabilities, the parameters are set as follows: the sampling frequency is $f_s = 10.23$ MHz, the sampling points is 2×10^7, the GPS direct wave power is $P_d = -100$ dBm, the symbol rate is $f_{Gb} = 1.023$ MHz, the carrier frequency is $f_c = 1.57$ GHz, the aerial target flight altitude is 10 km, the flight speed is 100 m/s, the average power of the echo signal is $P_r = -135$ dBm; 2000 Monte Carlo simulation results are used.

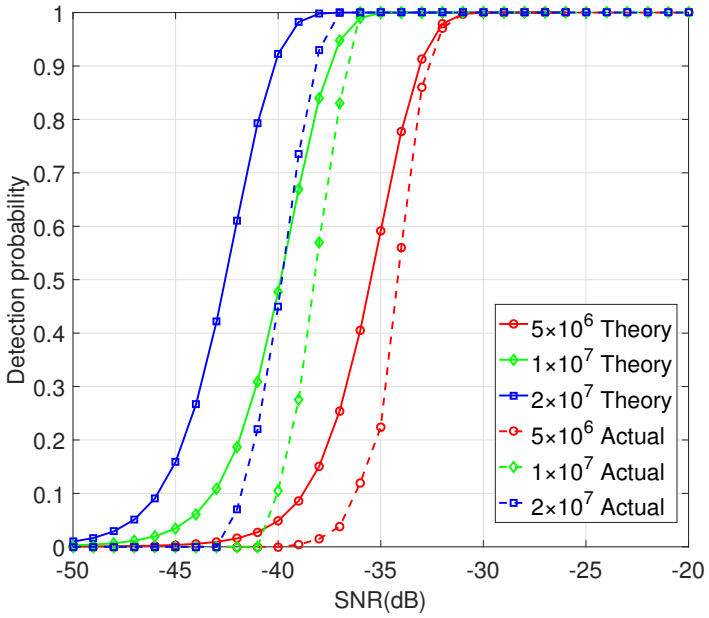

Figure 12. Sensing performance with different sampling points.

It can be seen in Figure 13 that, as the false alarm probability increases, so does the target sensing performance under the same conditions. When the false alarm probability is 10^{-4}, the sensing performance can reach 100% with SNR = -37 dB, and when the false alarm probability is 10^{-5}, the sensing performance under SNR = -35 dB can reach 100%,

and when the false alarm probability is 10^{-6}, the sensing performance can reach 100% with SNR = -34 dB.

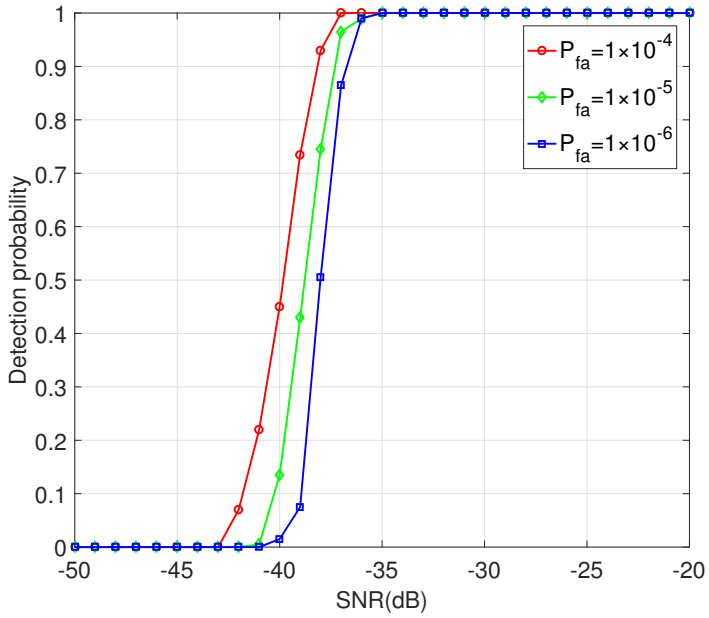

Figure 13. Sensing performance with different false alarm probabilities.

Next, we compare the target sensing performance of the proposed method with these of [32,33]. The parameters are set as follows: the sampling frequency is $f_s = 10.23$ MHz, the sampling points is 2×10^7, the false alarm probability is $P_{fa} = 10^{-4}$, the GPS direct wave power is $P_d = -100$ dBm, the symbol rate is $f_{Gb} = 1.023$ MHz, the carrier frequency is $f_c = 1.57$ GHz, the aerial target flight altitude is 10 km, the flight speed is 100 m/s, the average power of the echo signal is $P_r = -135$ dBm; 2000 Monte Carlo simulations are used.

As can be seen from Figure 14, the sensing performance of the proposed method is better than [32,33]. This is because the proposed method based on LCT has a good interference suppression effect; therefore, under the same conditions, the detection amount of the proposed method is more conducive to the detection of target echoes, which is superior to the method proposed in [32]. The method proposed in [33] is based on the shadow area in the case of forward scattering, but as the height of the target increases, its attenuation at the baseline decreases, which is not conducive to target detection. The computational complexity of the proposed method is $O(NM \cdot n_{lct})$, and the computational complexity of [32] method is $O(Nm)$, and the computational complexity of [33] method is $O(N\log_2 N)$, where N denotes the number of signal sampling points, M stands for the number of sampling points in the linear canonical domain, and n_{lct} and m are the number of searches. Overall, although the computational complexity of the proposed method is higher than [32,33], the proposed method has better target sensing performance and multipath interference suppression effect.

In order to evaluate the target parameter estimation performance of the proposed method, the parameters are set as follows: the sampling frequency is $f_s = 10.23$ MHz, the sampling points is 3×10^7, the GPS direct wave power is $P_d = -100$ dBm, the symbol rate is $f_{Gb} = 1.023$ MHz, the carrier frequency is $f_c = 1.57$ GHz, the target flight altitude is 8 km, the flight speed is 125 m/s, the average power of the echo signal is $P_r = -135$ dBm; 2000 Monte Carlo simulation results are used.

As can be seen from Figure 15, both the proposed LCT+MF method and the proposed MF+LCT method in this paper can achieve good estimation performance for the target flight altitude, and they improve as the signal-to-noise ratio (SNR) increases. This is because the increase in the SNR makes the corresponding peaks during parameter estimation more

prominent, thereby improving the parameter estimation performance. The normalized minimum mean square error of the height estimation achieved by the LCT+MF method reaches 10^{-3} when SNR = -17 dB and the estimation performance of the MF+LCT method reaches 10^{-3} when SNR = -21 dB. From the above, the proposed methods have good estimation performance, which shows that the aerial target parameter estimation methods have good interference suppression effect.

From Figure 16, both the proposed LCT+MF method and the proposed MF+LCT method in this paper can achieve the good estimation performance of the target flight speed, and estimation performance improves as SNR increases. When SNR = -19 dB, the LCT+MF method and MF+LCT method can reach 10^{-3}, and the MF+LCT method is better than LCT+MF in the case of low SNR. These results show that the LCT algorithm has a good suppression effect on interference.

To compare the parameter estimation performance of the proposed method with [34], the parameters are set as follows: the sampling frequency is $f_s = 10.23$ MHz, the sampling points is 3×10^7, the GPS direct wave power is $P_d = -100$ dBm, the symbol rate is $f_{Gb} = 1.023$ MHz, the carrier frequency is $f_c = 1.57$ GHz, the target flight altitude is 8 km, the flight speed is 125 m/s, the average power of the echo signal is $P_r = -135$ dBm; 2000 Monte Carlo simulation results are used.

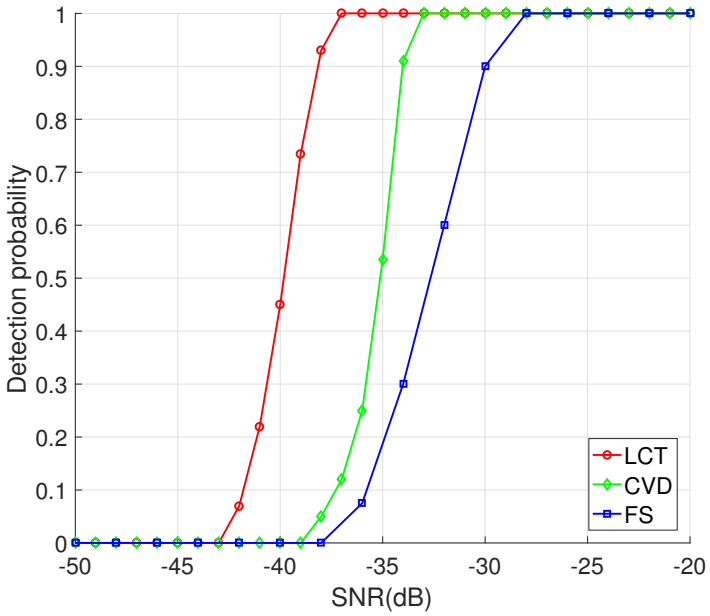

Figure 14. Sensing performance with different methods.

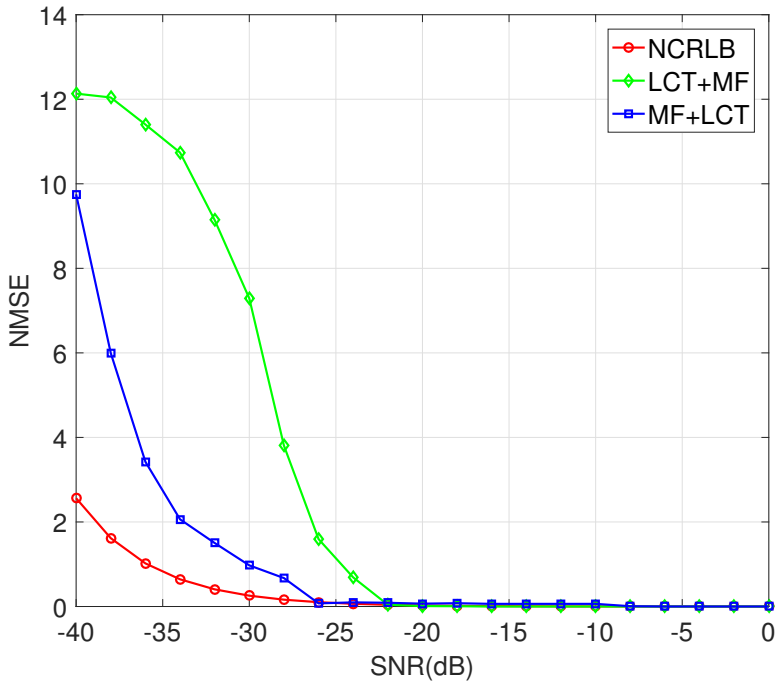

Figure 15. Height estimation performance with different SNRs.

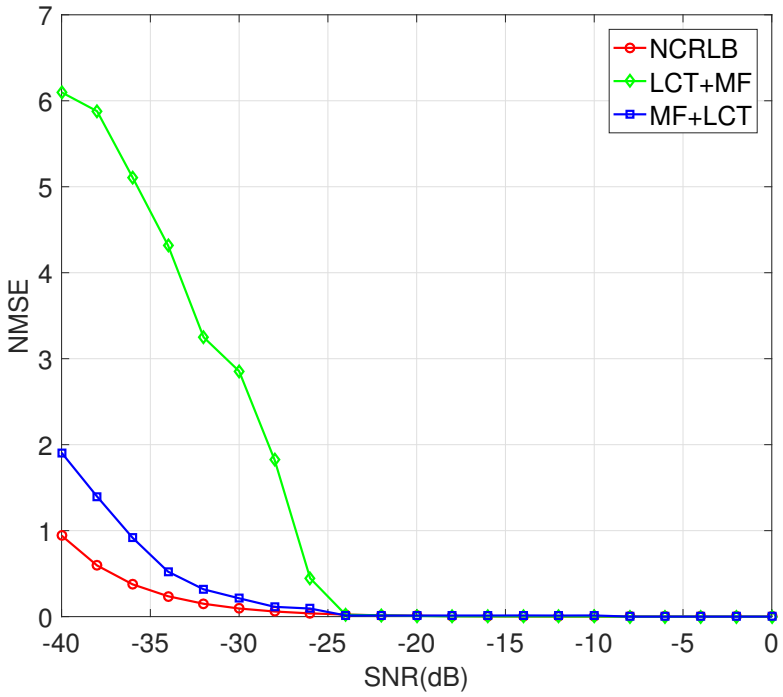

Figure 16. Speed estimation performance with different SNRs.

It can be seen from Figures 17 and 18 that the proposed method is better than [34]. This is because the proposed method completes the estimation of the target motion parameters based on the LCT based on the analysis of the forward scattered signal. The MF+LCT method and LCT+MF adopt the noise suppression effect of LCT and the time delay characteristics of the forward scattered signal, thus the proposed method has better estimation performance at low SNR. The computational complexity of the two methods are $O(MN \cdot n_{lct} + N \cdot n)$ and $O(MN \cdot n)$, respectively, and the computational complexity of [34] is $O(N \cdot n)$, where n is the total number of searches for speed and altitude. From the

above, although the computational complexity of the proposed methods is higher than [34], the proposed method can achieve better target parameter estimation performance.

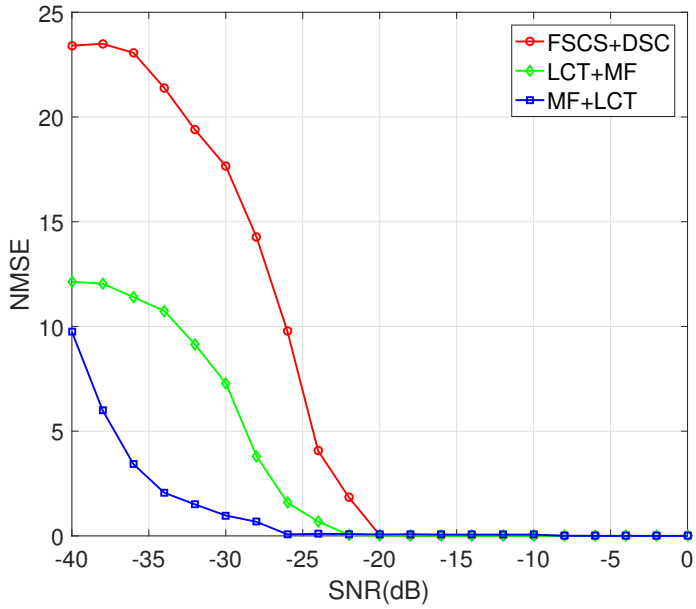

Figure 17. Height estimation performance with different methods.

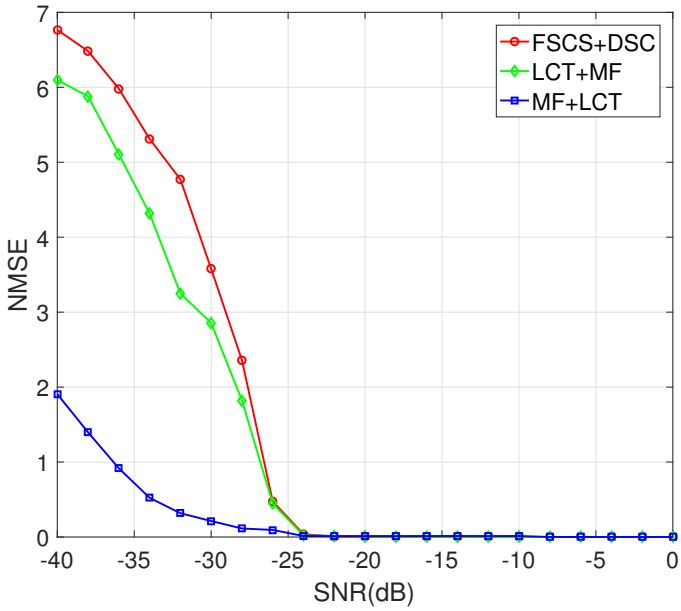

Figure 18. Speed estimation performance with different methods.

9. Conclusions

This paper has proposed a novel aerial target passive sensing method based on linear canonical transformation, in which the proposed method adopts the forward scatter radar model and satellite communication waveforms characteristics. Linear canonical transformation is used to achieve the multipath interference suppression in the receiving channel and design target detector. In addition, the characteristics of linear canonical and the matching filtering are used to achieve accurate target parameters estimate. Numerical results have demonstrated that the proposed method can perform effective target sensing and target parameter estimation by satellite based forward scatter radar. Satellite-based

target detection technology has become an important research direction in the field of passive detection. This paper has carried out a certain exploration in this field, but there are still other areas that can be further studied. In this paper, the research on GPS satellite target detection is based on theoretical modeling and computer simulation environment, and the actual environment and system model are simplified to some extent in the experiment. The proposed method can theoretically meet the needs of target detection, but in practice the working environment of target detection is more complicated; therefore, it is necessary to further connect with the actual environment, and carry out the verification and improvement of the algorithm and system through the measured data. In addition, since the suppression performance of direct wave interference and multipath interference will have a direct impact on the subsequent target detection and parameter estimation, it is necessary to further explore the improvement of the suppression performance of various interferences.

Author Contributions: M.L. conceptualized and performed the algorithm and wrote the paper; Z.Z. and S.Z. analyzed the experiment data; Y.C. helped improve the language; J.G. is the research supervisor. The manuscript was discussed by all co-authors. All authors have read and agreed to the published version of the manuscript.

Funding: This research was funded by the National Natural Science Foundation of China (62071364), the Aeronautical Science Foundation of China (2020Z073081001), the Fundamental Research Funds for the Central Universities (JB210104), the Shaanxi Provincial Key Research and Development Program (2019GY-043), and the 111 Project (B08038).

Institutional Review Board Statement: Not applicable.

Informed Consent Statement: Not applicable.

Data Availability Statement: Not applicable.

Conflicts of Interest: The authors declare no conflict of interest.

Appendix A

Proof of Lemma 1

In (24), the real part $\mathrm{Re}\{L(u)\}$ of the LCT under assumption H_1 is expressed as

$$\begin{aligned}\mathrm{Re}\{L(u)\} &= \mathrm{Re}\left\{\int_{-\frac{T}{2}}^{\frac{T}{2}} x(t)K_A(u,t)dt\right\}\\ &= \mathrm{Re}\left\{\int_{-\frac{T}{2}}^{\frac{T}{2}} A_T s_r(t)K_A(u,t)dt\right\}\\ &+ \mathrm{Re}\left\{\int_{-\frac{T}{2}}^{\frac{T}{2}} w(t)K_A(u,t)dt\right\}.\end{aligned} \tag{A1}$$

The first term of (A1) is the real part of the LCT of the echo signal, which belongs to the determined sensing statistics and is expressed as: $\mathrm{Re}\left\{\int_{-\frac{T}{2}}^{\frac{T}{2}} A_T s_r(t)K_A(u,t)dt\right\}$. The second term represents the real part of the LCT of noise, subject to Gaussian distribution, which is

$$\mathrm{Re}\left\{\int_{-\frac{T}{2}}^{\frac{T}{2}} w(t)K_A(u,t)dt\right\} \sim N\left(0,\sigma_{nn}^2\right). \tag{A2}$$

In summary, under the assumption H_1, $\mathrm{Re}\{L(u)\}$ subject to the Gaussian distribution of the following statistical characteristic

$$\mathrm{Re}\{L(u)\} \sim N\left(\mathrm{Re}\left\{\int_{-\frac{T}{2}}^{\frac{T}{2}} A_T s_r(t)K_A(u,t)dt\right\},\sigma_{nn}^2\right). \tag{A3}$$

In (25), the imaginary part $\mathrm{Im}\{L(u)\}$ of the LCT under assumption H_0 is expressed as

$$\begin{aligned}\mathrm{Im}\{L(u)\} &= \mathrm{Im}\left\{\int_{-\frac{T}{2}}^{\frac{T}{2}} x(t)K_A(u,t)dt\right\} \\ &= \mathrm{Im}\left\{\int_{-\frac{T}{2}}^{\frac{T}{2}} A_T s_r(t)K_A(u,t)dt\right\} \\ &+ \mathrm{Im}\left\{\int_{-\frac{T}{2}}^{\frac{T}{2}} w(t)K_A(u,t)dt\right\}.\end{aligned} \tag{A4}$$

Similarly, under the assumption H_1, $\mathrm{Im}\{L(u)\}$ follows a Gaussian distribution with

$$\mathrm{Im}\{L(u)\} \sim N\left(\mathrm{Im}\left\{\int_{-\frac{T}{2}}^{\frac{T}{2}} A_T s_r(t)K_A(u,t)dt\right\}, \sigma_{nn}^2\right). \tag{A5}$$

From (A3) and (A5), the distribution of the detection based on LCT under H_1 is

$$(l|H_1) \sim CN\left(\int_{-\frac{T}{2}}^{\frac{T}{2}} A_T s_r(t)K_A(u,t)dt, \sigma_{nn}^2\right), \tag{A6}$$

where $CN(\cdot)$ represents the complex Gaussian process.

In (24), the real part $\mathrm{Re}\{L(u)\}$ of the LCT under H_0 is expressed as

$$\begin{aligned}\mathrm{Re}\{L(u)\} &= \mathrm{Re}\left\{\int_{-\frac{T}{2}}^{\frac{T}{2}} x(t)K_A(u,t)dt\right\} \\ &= \mathrm{Re}\left\{\int_{-\frac{T}{2}}^{\frac{T}{2}} v(t)K_A(u,t)dt\right\},\end{aligned} \tag{A7}$$

where $\mathrm{Re}\{L(u)\}$ represents the real part of the LCT of noise, with

$$\mathrm{Re}\left\{\int_{-\frac{T}{2}}^{\frac{T}{2}} v(t)K_A(u,t)dt\right\} \sim NORM\left(0, \sigma_{nn}^2\right). \tag{A8}$$

In summary, under H_0, $\mathrm{Re}\{L(u)\}$ follows a Gaussian distribution with

$$\mathrm{Re}\{L(u)\} \sim N\left(0, \sigma_{nn}^2\right). \tag{A9}$$

In (25), the imaginary part $\mathrm{Im}\{L(u)\}$ of the LCT under H_0 is expressed as

$$\mathrm{Im}\{L(u)\} = \mathrm{Im}\left\{\int_{-\frac{T}{2}}^{\frac{T}{2}} w(t)K_A(u,t)dt\right\}. \tag{A10}$$

Similarly, under H_0, $\mathrm{Im}\{L(u)\}$ follows a Gaussian distribution with

$$\mathrm{Im}\{L(u)\} \sim N\left(0, \sigma_{nn}^2\right). \tag{A11}$$

From (A9) and (A11), the distribution of the sensing statistics based on LCT under the H_0 hypothesis is

$$(l|H_0) \sim CN\left(0, \sigma_{nn}^2\right). \tag{A12}$$

References

1. Garmatyuk, D. Cross-range SAR Reconstruction with Multicarrier OFDM Signals. *IEEE Geosci. Remote Sens. Lett.* **2012**, *9*, 808–812. [CrossRef]
2. Garmatyuk, D.; Simms, M.; Mudaliar, S. UWB Multicarrier Radar Target Scene Identification with 2-D Diversity Utilization and GLRT Refinement. *IEEE Sens. Lett.* **2019**, *3*, 1–5. [CrossRef]
3. Liu, M.; Li, K.; Song, H. Using Heterogeneous Satellites for Passive Detection of Moving Aerial Target. *Remote Sens.* **2020**, *12*, 1150. [CrossRef]
4. Wu, Q.; Xu, J.; Zeng, Y.; Ng, D.; Al-Dhahir, N.; Schober, R.; Swindlehurst, A. A comprehensive overview on 5G-and-beyond networks with UAVs: From communications to sensing and intelligence. *IEEE J. Sel. Areas Commun.* **2021**, *39*, 2912–2945. [CrossRef]
5. Hu, C.; Antoniou, M.; Cherniakov, M.; Sizov, V. Quasi-optimal signal processing in ground Forward Scattering Radar. In Proceedings of the 2008 IEEE Radar Conference, Rome, Italy, 26–30 May 2008; pp. 1–6.
6. Blyakhman, A.B.; Burov, V.N.; Myakinkov, A.V.; Ryndyk, A.G. Detection of unmanned aerial vehicles via multi-static forward scattering radar with airborne transmit positions. In Proceedings of the 2014 International Radar Conference, Lille, France, 13–17 October 2014; pp. 1–5.
7. Blyakhman, A.; Runova, I. Forward scattering radiolocation bistatic RCS and target detection. In Proceedings of the IEEE International Radar Conference, Waltham, MA, USA, 22–22 April 1999; pp. 203–208.
8. Myakinkov, A. Optimal detection of high-velocity targets in forward scattering radar. In Proceedings of the 5th International Conference on Antenna Theory and Techniques, Kyiv, Ukraine, 24–27 May 2005; pp. 345–347.
9. Myakinkov, A.; Ryndyk, A. Space-time processing in three-dimensional forward scattering radar. In Proceedings of the 4th International Conference on Antenna Theory and Techniques, Sevastopol, Ukraine, 9–12 September 2003; pp. 355–358.
10. Blyakhman, A.; Ryndyk, A.; Sidorov, S. Forward scattering radar moving object coordinate measurement. In Proceedings of the IEEE International Radar Conference, Alexandria, VA, USA, 12 May 2000; pp. 678–682.
11. Cherniakov, M.; Abdullah, R.R.; Jančovič, P.; Salous, M.; Chapursky, V. Automatic ground target classification using forward scattering radar. *IEE-Proc.-Radar Sonar Navig.* **2006**, *153*, 427–437. [CrossRef]
12. Gashinova, M.; Daniel, L.; Sizov, V.; Hoare, E.; Cherniakov, M. Phenomenology of doppler forward scatter radar for surface targets observation. *IET Radar Sonar Navig.* **2013**, *7*, 422–432. [CrossRef]
13. Wang, Z.; Du, L.; Mao, J.; Liu, B.; Yang, D. SAR target detection based on SSD with data augmentation and transfer learning. *IEEE Geosci. Remote Sens. Lett.* **2018**, *16*, 150–154. [CrossRef]
14. Zhong, C.; Mu, X.; He, X.; Wang, J.; Zhu, M. SAR target image classification based on transfer learning and model compression. *IEEE Geosci. Remote Sens. Lett.* **2018**, *16*, 412–416. [CrossRef]
15. Lu, C.; Li, W. Ship classification in high-resolution SAR images via transfer learning with small training dataset. *Sensors* **2019**, *19*, 63. [CrossRef] [PubMed]
16. Rostami, M.; Kolouri, S.; Eaton, E.; Kim, K. Deep transfer learning for few-shot SAR image classification. *Remote Sens.* **2019**, *11*, 1374. [CrossRef]
17. Suberviola, I.; Mayordomo, I.; Mendizabal, J. Experimental results of air target detection with a GPS forward-scattering radar. *IEEE Geosci. Remote Sens. Lett.* **2012**, *9*, 47–51. [CrossRef]
18. Vera, B.; Christo, K. Detectability of air targets using bistatic radar based on GPS L5 signals. In Proceedings of the 2011 12th International Radar Symposium, Leipzig, Germany, 7–9 September 2011; pp. 212–217.
19. Vera, B.; Christo, K. Air target detection using navigation receivers based on GPS L5 signals. In Proceedings of the 2011 24th International Technical Meeting of the Satellite Division of the Institute of Navigation, Portland, OR, USA, 20–23 September 2011; pp. 333–337.
20. Wachtl, S.; Koch, V.; Schmidt, L.P. Multipath sensor based on GNSS for passive airborne surveillance. In Proceedings of the 2013 European Radar Conference, Nuremberg, Germany, 9–11 October 2013; pp. 255–258.
21. Liu, C.; Hu, C.; Zeng, T.; Wang, L.; Long, T. Signal modeling and experimental verification in GNSS forward scatter radar. In Proceedings of the International Radar Symposium, Krakow, Poland, 10–12 May 2016; pp. 1–6.
22. Hu, C.; Wang, L.; Liu, C. SISAR imaging method based on GNSS signal: Theory and experimental results. In Proceedings of the 2016 CIE International Conference on Radar, Guangzhou, China, 10–13 October 2016; pp. 1–5.
23. Sithiravel, R.; Balaji, B.; Nelson, B.; McDonald, M.; Tharmarasa, R.; Kirubarajan, T. Airborne maritime surveillance using magnetic anomaly detection signature. *IEEE Trans. Aerosp. Electron. Syst.* **2020**, *56*, 3476–3490. [CrossRef]
24. Azemati, A.; Moghaddam, M.; Bhat, A. Bistatic scattering forward model validation using GNSS-R observations. In Proceedings of the 2019 IEEE International Geoscience and Remote Sensing Symposium, Yokohama, Japan, 28 July–2 August 2019; pp. 5964–5967.
25. Zhang, Z.; Li, D.; Chen, Y.; Zhang, J. Linear canonical wigner distribution of noisy LFM signals via multiobjective optimization analysis involving variance-SNR. *IEEE Commun. Lett.* **2021**, *25*, 546–550. [CrossRef]
26. Liu, M.; Gao, Z.; Chen, Y. Passive Detection of Moving Aerial Target Based on Multiple Collaborative GPS Satellites. *Remote Sens.* **2020**, *12*, 263. [CrossRef]
27. Murray, J. On the doppler bias of hyperbolic frequency modulation matched filter time of arrival estimates. *IEEE J. Ocean. Eng.* **2019**, *44*, 446–450. [CrossRef]

28. McPhee, H.; Ortega, L.; Vilĺd'-Valls, J.; Chaumette, E. On the accuracy limit of joint time-delay/doppler/acceleration estimation with a band-limited signal. In Proceedings of the 2021 IEEE International Conference on Acoustics, Speech and Signal Processing, Toronto, ON, Canada, 6–11 June 2021; pp. 5130–5134.
29. Liu, M.; Li, B.; Chen, Y.; Yang, Z.; Zhao, N.; Liu, P.; Gong, F. Location parameter estimation of moving aerial target in space-air-ground integrated networks-based IoV. *IEEE Internet Things J.* **2021**. [CrossRef]
30. Liu, M.; Liu, Z.; Lu, W.; Chen, Y.; Gao, X.; Zhao, N. Distributed Few-Shot Learning for Intelligent Recognition of Communication Jamming. *IEEE J. Sel. Top. Signal Process.* **2021**. [CrossRef]
31. Liu, M.; Liu, C.; Li, M.; Chen, Y.; Zheng, S.; Zhao, N. Intelligent passive detection of aerial target in space-air-ground integrated networks. *China Commun.* **2022**, *19*, 52–63. [CrossRef]
32. Ustalli, N.; Lombardo, P.; Pastina, D. Detection performance of a forward scatter radar using a crystal video detector. *IEEE Trans. Aerosp. Electron. Syst.* **2018**, *54*, 1093–1114. [CrossRef]
33. Kabakchiev, C.; Garvanov, I.; Behar, V.; Kabakchieva, D.; Kabakchiev, K.; Rohling, H.; Kulpa, K.; Yarovoy, A. Detection and classification of objects from their radio shadows of GPS signals. In Proceedings of the 2015 16th International Radar Symposium, Dresden, Germany, 24–26 June 2015; pp. 906–911.
34. De Luca, A.; Daniel, L.; Gashinova, M.; Cherniakov, M. Target parameter estimation in moving transmitter moving receiver forward scatter radar. In Proceedings of the 2017 18th International Radar Symposium, Prague, Czech Republic, 28–30 June 2017; pp. 1–7.